Journal of Alloys and Compounds 504S (2010) S91–S94

Contents lists available at ScienceDirect

Journal of Alloys and Compounds

journal homepage: www.elsevier.com/locate/jallcom

Nanocrystallization in $Al_{85}Ce_8Ni_5Co_2$ amorphous alloy obtained by different strain rate during high pressure torsion

P. Henits[a], Zs. Kovács[a,b], E. Schafler[c], L.K. Varga[d], J.L. Lábár[a,e], Á. Révész[a,*]

[a] Department of Materials Physics, Eötvös University, Budapest, H-1518, P.O.B. 32, Budapest, Hungary
[b] School of Electrical, Electronic & Mech. Engineering, Univ. College Dublin, Belfield, Dublin 4, Ireland
[c] Physics of Nanostructured Materials, Faculty of Physics, University of Vienna, A-1090 Vienna, Austria
[d] Research Inst. for Solid State Physics and Optics, Hungarian Academy of Sciences, Budapest, Hungary
[e] Research Inst. for Technical Physics and Mater. Science, Hungarian Academy of Sciences, Budapest, Hungary

ARTICLE INFO

Article history:
Received 2 July 2009
Received in revised form 7 January 2010
Accepted 18 March 2010
Available online 23 March 2010

Keywords:
Metallic glasses
Precipitation
Crystal growth

ABSTRACT

In order to elucidate the role of total strain and strain rate during high pressure torsion of $Al_{85}Ce_8Ni_5Co_2$ metallic glass, different deformation conditions were applied to devitrify the as-quenched alloy. The disk-shaped specimens were characterized by X-ray diffraction, transmission electron microscopy and thermal analysis.

1. Introduction

Single phase amorphous Al-based aluminium–transition-metal–rare-earth alloys (Al–TM–RE) have successfully been synthesized over a wide composition range in the last decades [1]. An extensive survey on the crystallization of these alloys has been proceeded, because of the superior mechanical properties, associated with the primary precipitation of fcc-Al nanocrystals in the residual amorphous matrix [2]. According to the λ topological instability criterion [3] and the Δx electronegativity differences among the constituent elements, Al–TM–RE glass formers can be grouped into three categories, reflecting to different thermal and crystallization features: nanocrystalline, glassy and nanoglassy [4,5].

Apart from heat-induced crystallization, deformation can also promote nanocrystallization in certain amorphous Al-based systems [6–10], however, the role of composition, thermodynamics and crystal growth kinetics has not been elucidated unambiguously. In a recent work we suggested that the growth of the crystalline nuclei is determined by the available free volume fluctuations [11]. Interestingly, similarities between deformation and irradiation induced crystallization have been found, indicating the importance of stability of the developing crystalline phases against irradiation [12].

In a recent study it was shown that $Al_{85}Ce_8Ni_5Co_2$ amorphous alloy exhibits eutectic crystallization after a clearly resolved glass transition [13], in line with $\lambda = 0.109 > 0.1$ and $\Delta x = 0.154 > 0.135$–0.145, corresponding to glassy nature [4,5]. On contrary, during extreme deformation obtained by high pressure torsion (HPT), the devitrification starts with the primary precipitation of Al nanocrystals [8].

In the present work, we investigate in detail the role of the strain and strain rate on the growth kinetics and stability of the nucleating crystalline phases during HPT of amorphous $Al_{85}Ce_8Ni_5Co_2$ alloy.

2. Experimental

Ingot of $Al_{85}Ce_8Ni_5Co_2$ was synthesized by induction melting of a mixture of high purity (99.9%) Al, Ce, Ni and Co metals. Fully amorphous ribbon sample was obtained using a single roller melt spinning technique in inert atmosphere. The as-quenched ribbon was cut into small pieces (flakes), pre-compacted and then deformed between anvils of the HPT device resulting in porosity free disks with a radius of $R = 5$ mm and thickness of $L = 0.7$ mm. The torsion straining was performed under different conditions, i.e., $f = 1$ revolution/min for $N = 5$ whole turns (5 rot@1 min^{-1}), $f = 0.2$ revolution/min for $N = 5$ whole turns (5 rot@0.2 min^{-1}), $f = 0.2$ revolution/min for $N = 1$ whole turn (1 rot@0.2 min^{-1}). The shear strain and strain rate for torsion deformation at a radius r can be represented by $\gamma(r) = 2r\pi N/L$ and $d\gamma(r)/dt = 2rf/L$, respectively. For sample 5 rot@1 min^{-1} the calculated values are $\gamma(R) \approx 220$ and $d\gamma(R)/dt \approx 0.7\ s^{-1}$.

Local area X-ray diffraction (XRD) measurements were carried out on a high resolution double crystal diffractometer with negligible instrumental broadening equipped with a fine focus rotating copper anode (Nonius, FR 591) operating at 45 kV and 80 mA. The symmetrical Ge (2 2 0) primary monochromator produced monochromatic Cu Kα radiation. The spot size of the X-ray beam on the specimen was 100 μm × 500 μm. Diffraction patterns were registered by FUJI Imaging Plate (BAS MS2025).

* Corresponding author. Tel.: +36 1 372 2823; fax: +36 1 372 2811.
E-mail address: reveszadam@ludens.elte.hu (Á. Révész).

0925-8388/$ – see front matter © 2010 Elsevier B.V. All rights reserved.
doi:10.1016/j.jallcom.2010.03.145

For transmission electron microscopy (TEM), parts of the HPT disks were prepared by twin-jet electropolishing (Tenupol-5) in a solution of water, ethanol, butoxyethanol and 1/78 ml perchloric acid (Struers A2 Electrolyte). The thin part of the sample around the perforation was investigated in a JEOL FX 2010 TEM at 200 keV. Standard dark-field (DF) images were recorded in "plane view" of the HPT disk together with selected area electron diffraction patterns (SAED).

Continuous thermal scans at 40 K/min were carried out in a PerkinElmer power compensated differential scanning calorimeter (DSC), under purified argon atmosphere. The temperature and enthalpy were calibrated by using pure Al and In.

3. Results and discussion

A general view of the effect of the external deformation parameters on the microstructure of the HPT disks can be inferred from Figs. 1 and 2. The XRD pattern corresponding to the as-quenched alloy exhibits featureless halo corresponding to fully amorphous nature (Fig. 1). The diffractogram of the centre of the 1 rot@0.2 min^{-1} sample shows weak diffraction peaks of fcc-Al superimposed on the amorphous halo. Applying the same rate up to 5 whole rotations some new crystalline peaks emerged identified as $Al_{11}Ce_3$ besides the fcc-Al peaks. On contrary, increasing the strain rate significantly (5 rot@1 min^{-1}), no detectable crystallization occurs in the central region of the disk. The XRD patterns obtained on the edge of the HPT disks results in a slight increase of peak intensity for disks processed by the lower strain rate, whereas noticeable crystallization of fcc-Al nanocrystals takes place in the perimeter of the disk at higher strain rates.

Fig. 2 summarizes the TEM analysis obtained on the edge of the different disks. The typical SAED pattern of the 1 rot@0.2 min^{-1} sample shows the amorphous halo with distinct faint crystalline spots (Fig. 2a). By analyzing these spots, it was found that they well fit on the diffraction rings of crystalline $Al_{11}Ce_3$ and fcc-Al. The DF image taken by one of the $Al_{11}Ce_3$ diffraction spots (see the circle) illustrates the formation of elongated particle with a length of 200 nm. The extremely low number of these intermetallic particles is in line with the absence of the $Al_{11}Ce_3$ Bragg peaks in the corresponding XRD pattern (see Fig. 1). At the same time, the density of Al nanocrystals (10 nm) is also very small (not shown here). As the revolution number increases up to 5, the SAED pattern is still dominated by diffuse halos, indicating that the amorphous state is present in large volumes, however, the density of the crystalline spots on the SAED pattern of the partially crystalline regions increases (see Fig. 2b). The DF image reveals well defined $Al_{11}Ce_3$ blocks with a size of 400 nm. It noted that the SAED pattern taken on an Al diffraction spot still shows small nanocrystals with slightly higher density distributed more homogeneously than the $Al_{11}Ce_3$ blocks in the amorphous matrix (not shown here). The SAED pattern of the sample 5 rot@1 min^{-1} consists of a halo with some faint diffraction rings of fcc-Al phase (see Fig. 2c), in accordance with the XRD results. The corresponding DF image taken by part of the (1 1 1) fcc-Al diffraction ring reveals that the Al nanocrystallites with a size of 5–10 nm are abundantly and homogeneously distributed in the residual amorphous matrix.

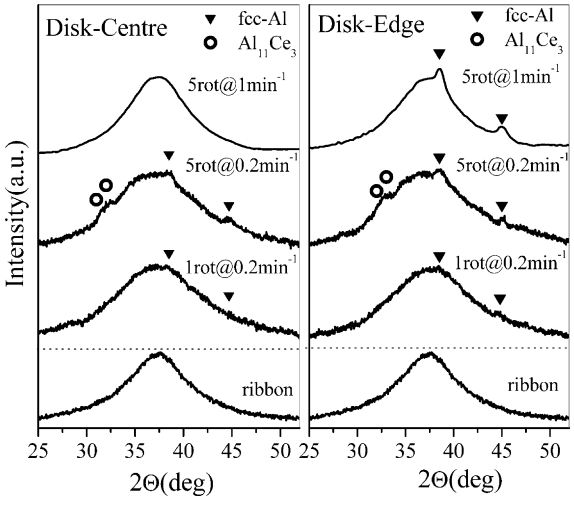

Fig. 1. XRD patterns of the as-quenched amorphous $Al_{85}Ce_8Ni_5Co_2$ alloy and the centre and edge of the HPT disks performed under different conditions. For the abbreviations, see the text.

As seen in Fig. 3, the as-quenched $Al_{85}Ce_8Ni_5Co_2$ amorphous alloy exhibits a two-stage thermal devitrification process characterized by the T_1 and T_2 crystallization peaks. Before the crystallization, the DSC thermogram also reveals a well defined glass transition (T_g). The inner part of the disks performed at the lower angular speed (0.2 min^{-1}) has similar thermal characteristics. However, when the strain rate is larger (1 min^{-1}), a high temperature thermal event (T_3) also appears. If we have a closer look on the effect of strain (i.e. at the edge of the disks), it is noticed that the magnitude of the T_1 decreases for the disk performed at 1 rot@0.2 min^{-1} and simultaneously a splitting of the T_2 peak occurs for 5 rot@0.2 min^{-1}. When the $Al_{85}Ce_8Ni_5Co_2$ alloy is subjected to the larger deformation rate (5 rot@1 min^{-1}), the T_1 thermal event is completely eliminated, while the T_2 and T_3 peaks become much sharper. The total change of the DSC curves corresponds to the depletion of Al in the residual amorphous matrix resulting in a chemically different, but more stable amorphous structure [8].

The corresponding total enthalpy release (ΔH) determined from the thermograms is shown in Fig. 4. As seen, ΔH decreases by about 15–20% after the torsion deformation. For all states the heat release corresponding to edge of the disk is slightly lower than for the centre. In the case of 1 rot@0.2 min^{-1} and 5 rot@0.2 min^{-1} samples ΔH is practically the same, referring to similar crystalline volume fraction. The somewhat larger value of the 5 rot@1 min^{-1} alloy can be associated with the different crystalline products of different morphology.

Summarizing the experimental results, it is found that low strain rate (0.2 min^{-1}) devitrifies the fully amorphous $Al_{85}Ce_8Ni_5Co_2$ into the mixture of $Al_{11}Ce_3$ crystalline blocks and Al nanocrystals sparsely distributed in the amorphous matrix (Fig. 2b and c). On contrary, the much higher strain rate (5 rot@1 min^{-1}) promotes the formation of homogeneously distributed small Al nanoclusters (Fig. 2a). Similarly, homogenous nanocrystals were observed in nanoindentation around the indents [14,15]. Based on defect annihilation kinetics, Atzmon and co-workers has predicted that the number of nuclei decreases and the size of the nanocrystals increases with increasing strain rate [14]. In spite of the lower apparent strain rate, the presence of sub-micrometer blocks for samples 1 rot@0.2 min^{-1} and 5 rot@0.2 min^{-1} foresees extremely high atomic mobility and local strain rate in the vicinity of the crystals.

Based on a thermoplastic model involving thermal balance between the plastic work input and heat conduction during HPT, Hóbor et al. proposed that the temperature can reach T_g above a critical value of f [16]. Evidently, for smaller f, the average temperature increase is smaller and the deformation should be localized.

4. Conclusions

High pressure torsion of fully amorphous $Al_{85}Ce_8Ni_5Co_2$ at low strain rate devitrifies the matrix into the mixture of sparsely distributed $Al_{11}Ce_3$ crystalline blocks and Al nanocrystals. On other hand, high strain rate promotes only the formation of homogeneously distributed small Al nanoclusters and inhibits the growth of $Al_{11}Ce_3$.

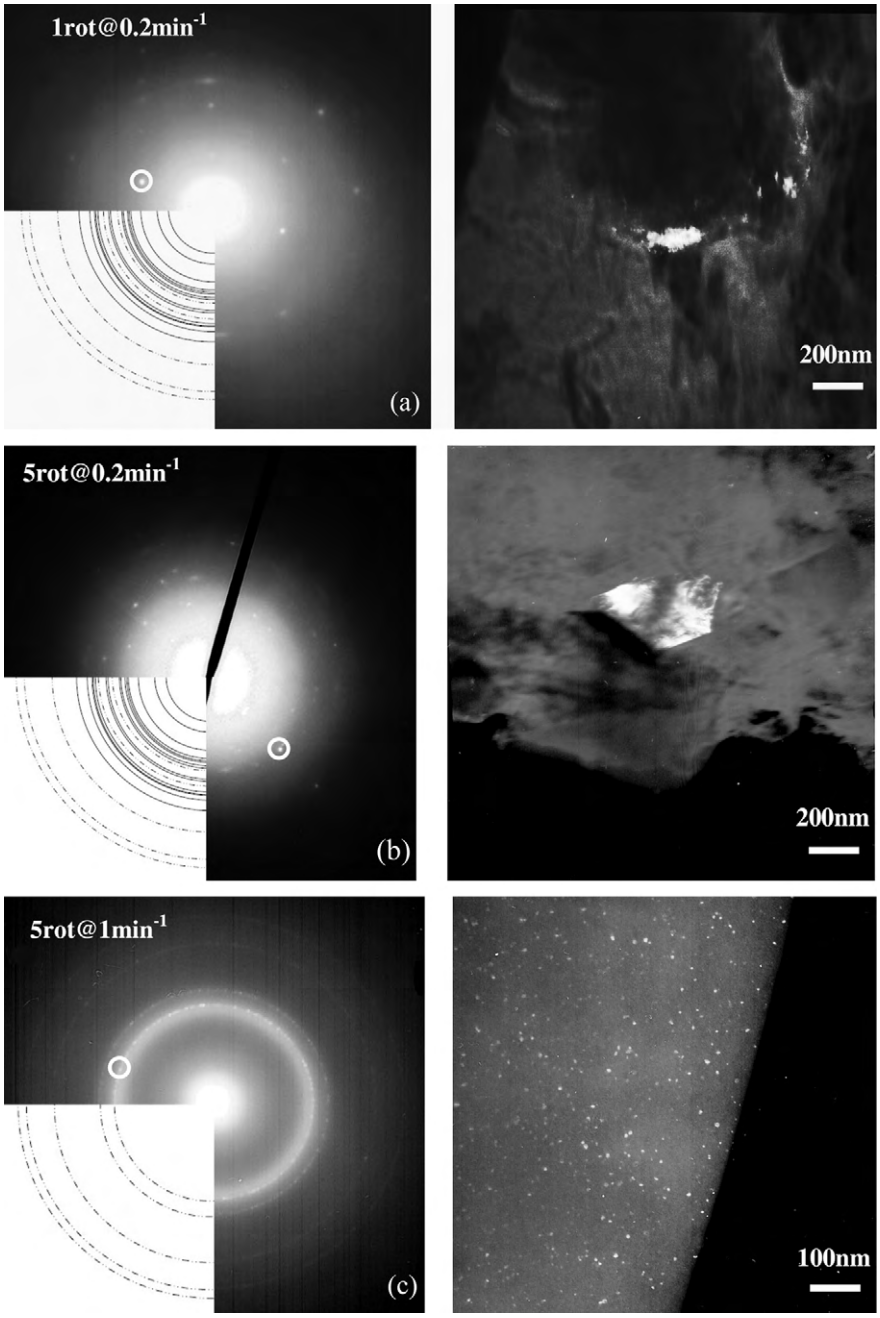

Fig. 2. SAED patterns and corresponding DF image of the HPT disks performed under different external conditions: (a) 1 rot@0.2 min^{-1}, (b) 1 rot@1 min^{-1} and (c) 5 rot@1 min^{-1}. Dashed and continuous rings correspond to fcc-Al and $Al_{11}Ce_3$, respectively.

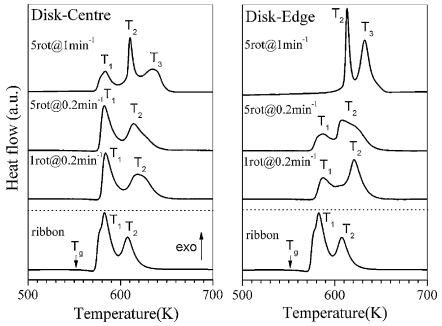

Fig. 3. DSC thermograms of the as-quenched amorphous $Al_{85}Ce_8Ni_5Co_2$ alloy and the centre and edge of the HPT disks performed under different conditions.

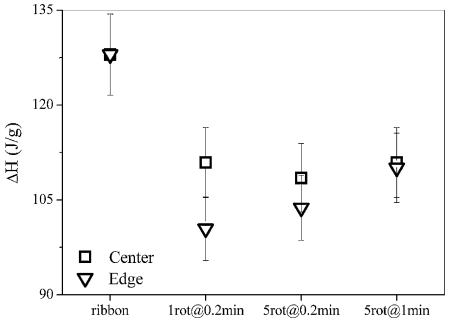

Fig. 4. Total enthalpy release (ΔH) obtained from the DSC curves for the as-quenched amorphous $Al_{85}Ce_8Ni_5Co_2$ alloy and the HPT disks performed under different conditions.

Acknowledgements

The authors acknowledge the Erich Schmid Institute of Material Science, Austria Academy of Science for providing the HPT facility. We appreciate the support of the Hungarian Scientific Research Fund under grant nos. F67893 and 67692. Á.R. is indebted for the János Bolyai Research Scholarship of the Hungarian Academy of Sciences. Zs.K. is grateful for the support of the Magyary Zoltán Fund and of the EEA Grants and Norway Grants.

References

[1] A. Inoue, Prog. Mater. Sci. 43 (1998) 365.
[2] Z.C. Zhong, X.Y. Jiang, A.L. Greer, Mater. Sci. Eng. A 226–228 (1997) 531.
[3] T. Egami, Y. Waseda, J. Non-Cryst. Solids 64 (1984) 113.
[4] R.D. Sá Lisboa, C. Bolifarini, W.J. Botta, C.S. Kiminami, Appl. Phys. Lett. 86 (2005) 211904.
[5] J.B. Fogagnolo, R.D. Sá Lisboa, C. Bolifarini, C.S. Kiminami, W.J. Botta, Phil. Mag. Lett. 88 (2008) 863.
[6] N. Boucharat, R. Hebert, H. Rösner, R. Valiev, G. Wilde, Scripta Mater. 53 (2005) 823.
[7] N. Boucharat, R. Hebert, H. Rösner, G. Wilde, High Pressure Technol. Nanomater. 114 (2006) 123.
[8] Zs. Kovács, P. Henits, A.P. Zhylaev, Á. Révész, Scripta Mater. 54 (2006) 1733.
[9] R.J. Hebert, J.H. Perepezko, Met. Mater. Trans. A 39 (2008) 1804.
[10] W.H. Jiang, F.E. Pinkerton, M. Atzmon, Scripta Mater. 48 (2003) 1195.
[11] P. Henits, Á. Révész, L.K. Varga, Zs. Kovács, Intermetallics, submitted.
[12] W. Qin, T. Nagase, Y. Umakoshi, Acta Mater. 57 (2009) 1300.
[13] Á. Révész, L.K. Varga, S. Suriñach, M.D. Baró, J. Mater. Res. 17 (2002) 2140.
[14] W.H. Jiang, F.E. Pinkerton, M. Atzmon, J. Appl. Phys. 93 (2003) 9287.
[15] H. Chen, Y. He, G.J. Shiflet, S.J. Poon, Nature 367 (1994) 541.
[16] S. Hóbor, Zs. Kovács, Á. Révész, J. Appl. Phys. 106 (2009) 023531.